Journal of Artificial Intelligence Practice (2024)
Clausius Scientific Press, Canada

DOI: 10.23977/jaip.2024.070118
ISSN 2371-8412 Vol. 7 Num. 1

Research on Cloud Detection in Non-agricultural Image Based on Long Time Series Data

Ping Wu[1,a,*], Xiaoping Lin[1]

[1]*Fujian Provincial Natural Resources Geographic Information Center, Fuzhou, Fujian, 350003, China*
[a]*76991857@qq.com*
[*]*Corresponding author*

Keywords: Long-Time Series Data, Non-Agriculturalization, Remote Sensing Imagery, Cloud Detection

Abstract: With the rapid development of China's economy, the increasingly severe phenomenon of farmland non-agriculturalization may potentially impact China's food security. Against this backdrop, the task of monitoring farmland non-agriculturalization in Fujian Province has become increasingly arduous, leading to an exponential increase in the amount of remote sensing image data that needs to be received and analyzed throughout the year. Solely relying on manual methods for analyzing the quality of vast amounts of data becomes highly challenging. Therefore, it is imperative to introduce automated detection technology to improve the speed of cloud layer detection in images. This paper proposes an algorithm that utilizes long-term historical sequences of remote sensing imagery to obtain statistical data on the dark channel prior of ground objects, which are then compared with the dark channel prior from the images to be inspected, thereby obtaining information about cloud layers. Experimental validation confirms that the method presented in this paper can achieve automatic cloud layer detection, which to a certain extent improves production efficiency while also delivering relatively satisfactory detection results.

1. Introduction

Agricultural land is a vital foundation and safeguard for China's food security. With the rapid economic development in our country, the phenomenon of farmland non-agriculturalization has been increasingly exacerbated. This trend, on one hand, promotes economic growth, but on the other hand, it poses certain negative impacts on food security, social stability, and ecological environment. In response to the pressing demand for monitoring farmland non-agriculturalization in Fujian Province, satellite remote sensing monitoring serves as a significant technological means to quickly, efficiently, objectively, and accurately monitor scenarios such as illegal occupation of farmland for non-agricultural construction activities in Fujian province [1-4]. With the swift advancement of domestically produced satellite technology, the frequency of non-agriculturalization satellite remote sensing monitoring in our province has continuously increased, transitioning from an annual full coverage monitoring once a year to a primary focus on

"quarterly and annual" monitoring, and further evolving into a stage of "monthly clearance, quarterly verification, and annual assessment". This progression leads to an exponential increase in the volume of remotely sensed image data that needs to be received and analyzed throughout the year. Given these circumstances, this paper proposes a cloud cover detection technique based on long-term sequence historical remote sensing image data for monitoring farmland non-agriculturalization in Fujian province. The aim is to automate the process of detecting cloud cover in monitoring images, thereby reducing manual workload and enhancing production efficiency.

2. Algorithm Design

2.1 Algorithm Flow

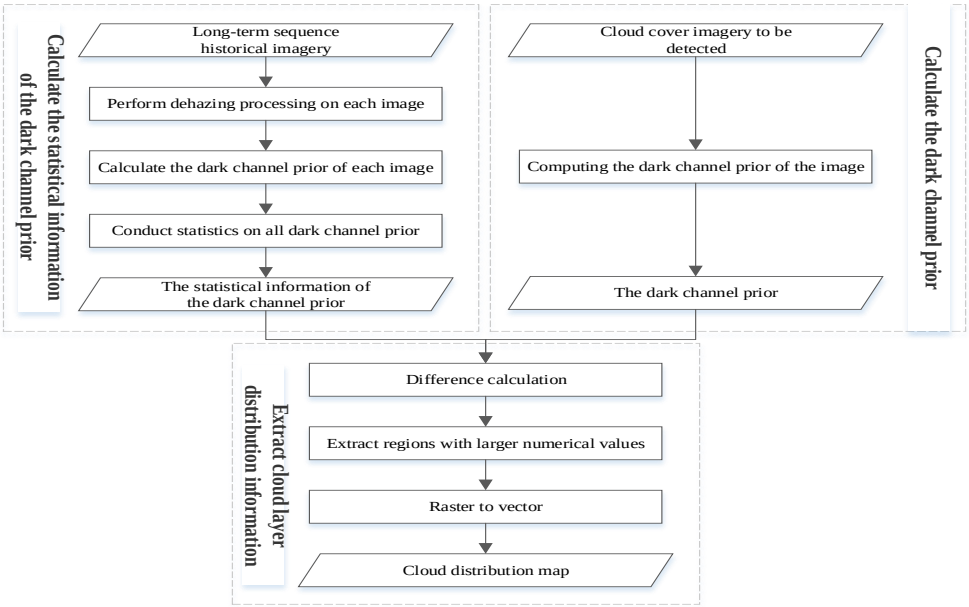

Figure 1: The flowchart of the algorithm

Currently, the amount of various remote sensing image data received in Fujian province has reached 20 TB, achieving multi-round coverage across the entire province in terms of distribution, with spatial resolutions ranging from 0.5 meter to 2.5 meter for various medium-resolution to high-resolution images, and the earliest dating back to 1998. Within this massive volume of data, there exists a wealth of latent correlation information among the points of the same feature objects, meaning that these points should exhibit similar spectral information on different images. However, when an object is obscured by cloud cover, its spectral information will undergo significant changes compared to when no clouds are present. The dark channel prior, which is a higher-order information derived from spectral information, also experiences similar changes. Therefore, it is possible to use these potential relationships among the points of the same feature objects in long-time series image data to detect cloud. This method is based on dark channel prior technology, using the difference between the statistical information of dark channel prior in the long-time series image data and the statistical information of the dark channel prior in the image to be detected to identify cloud layers. The specific steps are as follows: First, calculate the statistical information of the dark channel prior by removing fog from the long-time series image data using a dark channel prior defogging method, then calculating the information of the dark channel prior for each processed image, and finally generating the statistical information map of the dark channel prior

through statistical analysis. Second, compute the dark channel prior for the image to be detected. Third, extract cloud distribution information by subtracting the information of the dark channel prior in the long-time series image data from the information of the dark channel prior of the image to be detected, obtaining a difference information. Identifying areas with larger values in this difference information allows for the extraction of cloud layer information. The flowchart of the algorithm is shown in Figure 1.

2.2 Calculate the Statistical Information of the Dark Channel Prior

2.2.1 Image defogging and dark channel prior computation

Dr. Kaiming He published the paper "Single Image Haze Removal Using Dark Channel Prior" in 2009 [5-8], proposing a technique for single image dehazing that utilizes the dark channel prior. In this technique, the dark channel is defined by identifying pixels within an image where the values across color channels are exceptionally low, which are then denoted as J_{dark}:

$$J_{dark}(x) = \min_{y\epsilon\Omega(x)} \left(\min_{c\epsilon\{r,g,b\}} J^c(y) \right) \tag{1}$$

In this context, J^c represents a particular color channel of the image J, and $\Omega(x)$ denotes a square region centered at point x. Equation (2) is used to estimate the approximate value $\tilde{t}(x)$ of the transmittance $t(x)$:

$$\tilde{t}(x) = 1 - \omega \min_{y\epsilon\Omega(x)} \left(\min_{c} \frac{J^c(y)}{A^c} \right) \tag{2}$$

Among them, $\min_{y\epsilon\Omega(x)} \left(\min_{c} \frac{J^c(y)}{A^c} \right)$ represents the dark channel prior of the normalized fog image $\frac{J^c(y)}{A^c}$, which directly provides transmission information. ω is a constant ($0 < \omega \ll 1$), used to selectively retain a portion of the fog that covers distant objects. By combining the fog degradation model [9-11], the original fog-free image can be restored, and the final restored image $J(x)$ is realized through the following formula:

$$J(x) = \frac{I(x) - A}{\max(t(x), t_0)} + A \tag{3}$$

Where t_0 is a lower limit value set for the transmission factor $t(x)$ to prevent noise from appearing in the restored original image. The global atmospheric light value A can be obtained from the hazy image using the dark channel map. By utilizing the aforementioned formula (1), we can calculate the dark primitive color information of both long-term historical image sequences and target cloud amount images, and at the same time, formula (3) can be used to perform dehazing processing on the long-term historical image sequences.

2.2.2 Statistical mean computation of dark channel information

After completing the dark channel information calculation for a long time series of historical images, it is necessary to statistically average these dark channel information pieces. The purpose of this is to provide a cloud-free reference baseline for subsequent comparisons. The specific method is as follows: Assuming that in a total of N images within the long time series historical imagery, the dark channel information for the nth image is denoted as D_n, then under ideal conditions, the statistical average of the dark channel information over the entire long time series historical imagery, represented by $\overline{D}$, would be:

$$\overline{D} = \frac{\sum_{n=1}^{N} D_n}{N} \tag{4}$$

However, considering that cloud cover also exists in historical images, during the calculation process, it is necessary to judge on a pixel-by-pixel basis whether an object is obscured by clouds. If a pixel is indeed obstructed by clouds, it should not be included in the statistical process. Add the following rules according to the above description:

$$\overline{D}_{ij} = \frac{\sum_{n=1}^{k} D_{ij}^{(n)}}{k} \quad (D_{ij}^{(n)} > d_0) \tag{5}$$

In this context, $\overline{D}_{ij}$ represents the pixel at coordinates (i, j) in $\overline{D}$, and $D_{ij}^{(n)}$ denotes the pixel at coordinates (i, j) in the nth image. d_0 is the brightness threshold used to determine whether a pixel belongs to a cloud. Since clouds appear dark in the dark channel prior, when $D_{ij}^{(n)}$ is greater than this threshold, it can be identified as a non-cloud area and thus participate in the statistical average calculation; otherwise, the pixel does not participate in the operation. k represents the total number of pixels that eventually take part in the calculation.

In addition, consideration should also be given to the fact that objects such as metal sheet houses can produce overexposed bright spots on images, which may be mistakenly identified as clouds and removed in the above-mentioned operations. Therefore, after completing the above calculations, appropriate rules need to be added to restore the regions that have been incorrectly removed. The specific method involves calculating the statistical average of dark primary color pixels under ideal conditions. If this average exceeds a preset brightness threshold, it can be determined that the pixel is a perennially high-reflective bright spot, and the value of this point should be replaced with the statistical average under ideal conditions as the final value. This can be represented mathematically as:

$$\overline{D}_{ij} = \begin{cases} \frac{\sum_{n=1}^{k} D_{ij}^{(n)}}{k} & (D_{ij}^{(n)} > d_0 \cap \frac{\sum_{n=1}^{N} D_{ij}^{(n)}}{N} \leq d_1) \\ \frac{\sum_{n=1}^{N} D_{ij}^{(n)}}{N} & (\frac{\sum_{n=1}^{N} D_{ij}^{(n)}}{N} > d_1) \end{cases} \tag{6}$$

Where d_1 represents the threshold for determining whether a pixel is a perennial highlight reflection point, and it's value should be greater than d_0. The result calculated through equation (6) is the final statistical average information of the dark channel prior.

2.3 Extracting Cloud Layer Distribution Information

After obtaining the statistical average information of the dark channel prior $\overline{D}$ and the dark channel prior D' from the image to be detected, subtract the two and extract the pixels with values greater than a specified threshold d_3. These points represent the locations of cloud-covered areas, which can be expressed mathematically as follows:

$$Y_{ij} = \begin{cases} 255 & (\overline{D}_{ij} - D'_{ij} > d_3) \\ 0 \end{cases} \tag{7}$$

In this context, D'_{ij} denotes the value at the point with coordinates (i, j) in the information of the dark channel prior, while Y_{ij} represents the pixel at the coordinates (i, j) within the cloud layer image. When the difference between these two values exceeds a predetermined threshold d_3 at any given point, that point is assigned a value of 255 to indicate cloud coverage; conversely, areas not covered by clouds are assigned a value of 0. Finally, after converting the image Y_{ij} into a vector

format, the extent of cloud coverage can be obtained.

3. Experimental Verification

The algorithm in this paper is implemented using Matlab software, and two sets of satellite remote sensing image data are selected for experiments to verify the effectiveness of the algorithm. As shown in Figure 2, the first set of experimental images includes Figures 2(a) through 2(e), which are historical images, while Figure 2(f) represents the image to be detected. Specific information about these images can be found in Table 1. From Table 1, it can be seen that the historical images encompass data from four different satellites and two resolutions, with a time span exceeding one year. In terms of image quality, the historical images include those affected by fog coverage and cloud occlusion, as well as higher-quality images. The experimental results are depicted in Figure 3, where the regions circled in red represent the final detection outcomes. It can be observed that the clouds on the image have basically been detected; however, a small portion of the clouds were not included in the final calculation because the algorithm determined they could potentially be removed using defogging techniques.

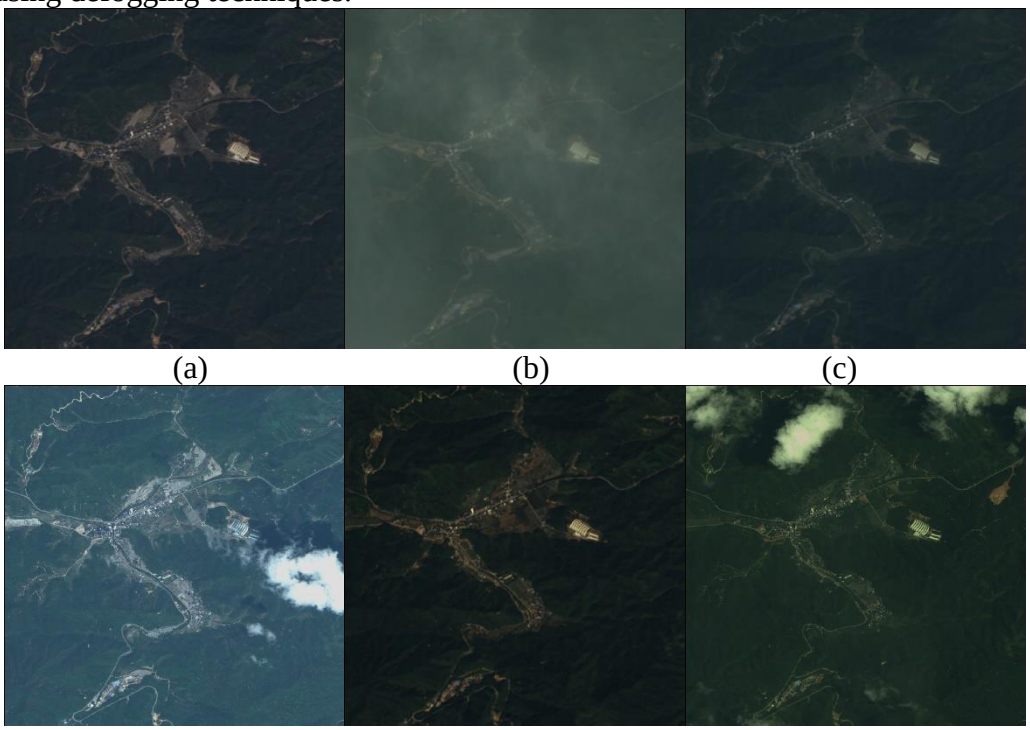

(a) (b) (c)

(d) (e) (f)

Figure 2: The first set of experimental images

Table 1: Detailed information of the first group of experimental images

Image	Satellite type	Resolution	Current situation	Remark
Fig. 2 (a)	GF-6	2 meters	May 1, 2021	Historical images
Fig. 2 (b)	GF-1	2 meters	March 2, 2022	Historical images
Fig. 2 (c)	GF-1	2 meters	April 7, 2022	Historical images
Fig. 2 (d)	GF-7	0.65 meters	July 11, 2022	Historical images
Fig. 2 (e)	CB-04	2 meters	October 11, 2022	Historical images
Fig. 2 (f)	BJ-3	0.8 meters	March 5, 2023	Image to be detected

Figure 3: Cloud detection results of the first group of images to be detected

The second set of experimental figures are shown in Figure 4, where Figures 4(a) to 4(e) represent historical images, and Figure 4(f) is the image under inspection. The specific information of these images can be found in Table 2. From Table 2, it can be seen that the historical images encompass data from five different satellites, three distinct resolutions, and cover a time span of nearly two years. In terms of image quality, historical images include both those with fog coverage and those of better quality. The experimental results are presented in Figure 5, where the regions circled by red vectors denote the final detection outcomes. It can be seen that the cloud layers on the image have also been basically detected.

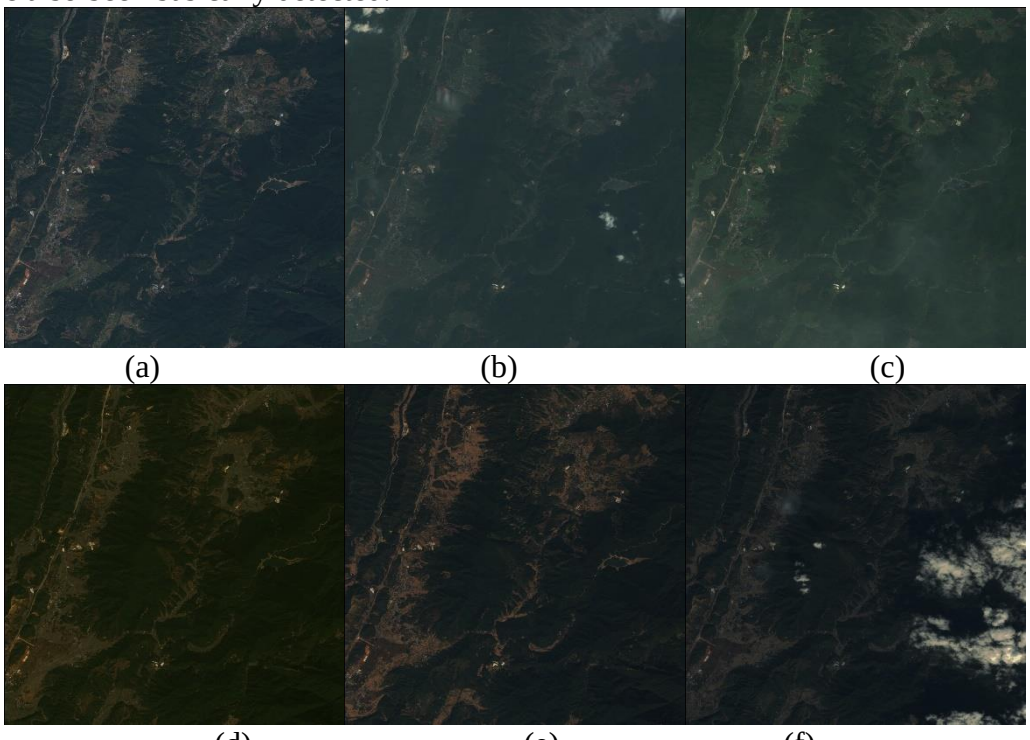

Figure 4: The second set of experimental images

Table 2: Detailed information of the second group of experimental images

Image	Satellite type	Resolution	Current situation	Remark
Fig. 4 (a)	CB-04	2 meters	December 26, 2020	Historical images
Fig. 4 (b)	GF-1	2 meters	April 12, 2021	Historical images
Fig. 4 (c)	ZY-3	2.1 meters	May 1, 2021	Historical images
Fig. 4 (d)	GF-6	2 meters	December 11, 2021	Historical images
Fig. 4 (e)	GF-7	0.65 meters	October 11, 2022	Historical images
Fig. 4 (f)	GF-1	2 meters	October 23, 2022	Image to be detected

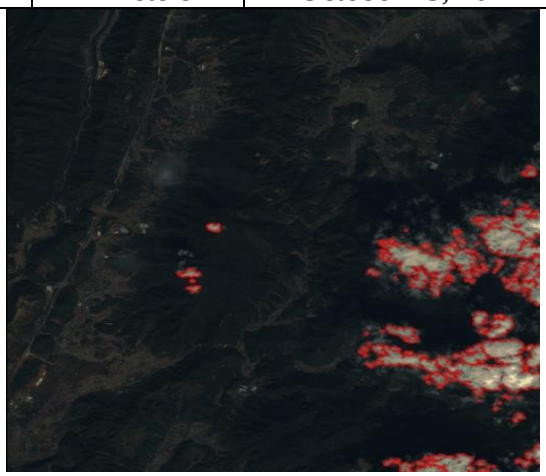

Figure 5: Cloud detection results of the second group of images to be detected

Through the above two sets of experiments, it can be seen that using this method can effectively detect cloud layers. The small portion of thin clouds that are not detected is mainly because they can be removed by defogging methods and thus were not identified as cloud layers. Overall, this method proves to be effective.

4. Conclusion

This paper employs long-term historical image data to detect cloud layers, and has verified the effectiveness of the method through experiments. The advantage of the algorithm lies in that it does not require a large amount of prior knowledge or pre-trained models; instead, satisfactory cloud detection results can be achieved by leveraging existing historical images alone. However, its disadvantage is that if there are substantial amounts of clouds or fog affecting the historical images, they may interfere with the construction of dark channel statistical information, thereby reducing the accuracy of cloud detection. For the aforementioned issues, we will continue to refine the algorithm in subsequent research, aiming to address these limitations.

Acknowledgements

This work was supported by Fujian Provincial Department of Natural Resources 2023 Science and Technology Innovation (Research on the Application of Long Term Sequence Multi source Remote Sensing Images, ID:K KY-100000-04-2023-008Y-100000-04-2023-008)

References

[1] Chen Fu, Zeng Siyan, Ge Xiaoping, et al. Identification of fallow priority areas in China under resource and environmental constraints. Journal of Agricultural Engineering, 2021, 37 (22): 226-235.

[2] Zhou Nan, Yang Peng, Wei Chunshan, et al. Method for precise extraction of cultivated land in mountainous area at block scale. Journal of Agricultural Engineering, 2021, 37 (19): 260-266.
[3] Yuan Xiaoni, Lu Chunyang, Lv Kaiyun, et al. Research progress and prospect of cultivated land conversion in China. China Agricultural Resources and Regionalization, 2019, 40 (1): 128-133.
[4] Li Fangting, Zhang Guo, Shi Tingting, et al. Classification system and application of remote sensing interpretation samples of cultivated land conversion. Journal of Agricultural Engineering, 2022, 38 (15): 297-304.
[5] Kaiming He, Jian Sun, and Xiaoou Tang. Single Image Haze Removal Using Dark Channel Prior. IEEE Transactions on Pattern Analysis and Machine Intelligence, 2011.
[6] You Qian. Research on the Clear Method of Fog Degraded Image. Kunming University of Science and Technology, 2013.
[7] Kong Qinghong. Research and implementation of UAV aerial image defogging algorithm based on dark channel prior. Ocean University of China, 2014.
[8] Fang Zhou. Research on Fog Image Clearing Method Based on Dark Primary Color Theory. Chongqing Jiaotong University, 2015.
[9] Fu Hui, Wu Bin, Li Linfei, et al. Haze image sharpness restoration based on dark primary prior. Computer Engineering, 2016, 42(7): 232-237.
[10] Wang Ping, Cheng Hao, Luo Yingxin. Color remote sensing image enhancement based on hue invariance. Chinese Journal of Image and Graphics, 2007, 12(7): 1173-1177.
[11] Li Guo, Zhang Jun, Gong Zhihui. Color preserving direct linear enhancement method for color remote sensing images. Geospatial Information, 2012, 10(5).